

Deep Learning-based Prediction of Key Performance Indicators for Electrical Machines

VIVEK PAREKH¹, DOMINIK FLORE², SEBASTIAN SCHÖPS³

¹Technische Universität Darmstadt, Computational Electromagnetics Group, Schloßgartenstrasse 8, 64289 Darmstadt and Robert Bosch GmbH, Powertrain Solutions, Mechanical Engineering and Reliability, 70442 Stuttgart (e-mail: Vivek.Parekh@de.bosch.com)

²Robert Bosch GmbH, Powertrain Solutions, Mechanical Engineering and Reliability, 70442 Stuttgart, Germany (e-mail: Dominik.Flore@de.bosch.com)

³Technische Universität Darmstadt, Computational Electromagnetics Group, Schlossgartenstrasse 8, 64289 Darmstadt, Germany (e-mail: sebastian.schoeps@tu-darmstadt.de)

Corresponding author: Vivek Parekh (e-mail: Vivek.Parekh@de.bosch.com).

arXiv:2012.11299v2 [cs.LG] 23 Jan 2021

ABSTRACT The design of an electrical machine can be quantified and evaluated by Key Performance Indicators (KPIs) such as maximum torque, critical field strength, costs of active parts, sound power, etc. Generally, cross-domain tool-chains are used to optimize all the KPIs from different domains (multi-objective optimization) by varying the given input parameters in the largest possible design space. This optimization process involves magneto-static finite element simulation to obtain these decisive KPIs. It makes the whole process a vehemently time-consuming computational task that counts on the availability of resources with the involvement of high computational cost. In this paper, a data-aided, deep learning-based meta-model is employed to predict the KPIs of an electrical machine quickly and with high accuracy to accelerate the full optimization process and reduce its computational costs. The focus is on analyzing various forms of input data that serve as a geometry representation of the machine. Namely, these are the cross-section image of the electrical machine that allows a very general description of the geometry relating to different topologies and the classical way of scalar geometry parametrizations. The impact of the resolution of the image is studied in detail. The results show a high prediction accuracy and proof that deep learning-based meta-models are able to minimize the optimization time. The results also indicate that the prediction quality of an image-based approach can be made comparable to the classical way based on scalar parameters.

INDEX TERMS Key Performance Indicators, meta-model, multi-objective optimization

I. INTRODUCTION

A. MOTIVATION

An electrical machine is a paramount part of an electrical drive. The automotive industry currently favors permanent magnet synchronous machines (PMSM) due to their numerous advantages like greater power density, high efficiency, broad speed range, large torque-current ratio etc., see for example [1]–[3]. Usually, the use of materials such as neodymium-iron-boron magnets, copper, and electrical steel makes a significant contribution to the cost of the electrical machine. Only the smaller part of the final cost is due to the added value. This is why numerical optimization of the active parts (rotor, magnets, stator, winding), i.e., minimizing material usage, can decrease the costs dramatically, before the

PMSM is manufactured. Especially when the design space (e.g. winding topology, current/voltage range, geometry parameter range, material parameter) is large. For PMSMs, a large design space requires approximately 50-100 input parameters, the impact of which must be evaluated and optimized for around 10-20 Key Performance Indicators (KPIs). In such a large design space, multi-objective optimization is very time consuming and thus cost-intensive if the use of finite element (FE) models is needed to extract the KPIs. Meta-models (also known as surrogate models, kriging) are often fed to the optimizer in order to overcome this and to adapt to continuously reduced development cycles in the automotive industry. This enables optimizations in a large design space in short time.

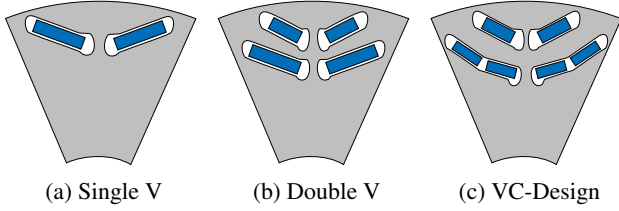


Figure 1: Different rotor topologies for PMSM

Another driver of this research work is to reuse simulation data or, in other words, to implement prior knowledge to a new optimization problem. Obviously, any optimization problem benefits if all the data (input parameters and output KPIs) of a previous problem were reused to direct the optimizer even faster into the optimal regions for the new problem. To date, transferring knowledge from one optimization to another is limited by the parametrization or the topology of an electrical machine. As shown in Figure 1 different topologies of electric machines can be used to perform parametric optimization. However, the parametrization varies greatly for each topology and so does the input of the corresponding meta-model. Hence, a more general geometry description, such as an image can be used to transfer knowledge from one optimization to another.

This paper investigates approaches to predict large numbers of KPIs of PMSM with a deep learning-based meta-model. It includes cross-domain KPIs, i.e. maximum torque, field strength, sound power level, cost of components, temperature level, etc. We address two questions. One is how accurately a classic scalar parameter-based meta-model can predict the KPIs with a given number of samples, and another is how the prediction accuracy of a more general and topology-invariant image-based meta-model performs (in dependency of the image resolution). To answer these questions, two datasets are used which vary in design parameters and KPIs with different distribution of input data.

The paper is structured as follows: section II briefly discusses the current state of the art in industrial simulation and optimization workflows. section III details of datasets and KPIs. section IV presents network architecture and training specifics. section V discuss the results and is followed by the conclusion.

II. STATE OF THE ART

Optimizing the design of an electrical machine involves cross-domain analysis, such as electromagnetic performance, stress and thermal behavior, etc., which essentially boils down to a multi-physics and multi-objective optimization (MOO) problem, e.g. [4]–[6]. To carry out MOO, various optimization approaches are outlined for example in [7]–[11].

A. MULTI-OBJECTIVE OPTIMIZATION

The design of an electrical machine shall be obtained by MOO; its goal functions are the (possibly conflicting) KPIs $y_j(\mathbf{p}) \in \mathbb{R}$ with $j = 1, \dots, n_y$, e.g. maximum torque,

maximum power, the tonality of a machine, torque ripple behavior, mass of the rotor, which depend on a parameter vector $\mathbf{p} \in \mathbb{R}^{n_p}$ (geometry, material and electrical excitation). This optimization problem can be abstractly written as

$$\min_{\mathbf{p}} y_j(\mathbf{p}), \quad j = 1, \dots, n_K \quad (1)$$

$$\text{s.t. } c_k(\mathbf{p}) \leq 0, \quad k = 1, \dots, n_c \quad (2)$$

where $c_k(\mathbf{p})$ may denote additional constraints, e.g. to avoid intersections of the geometry. The simulation and optimization chain is illustrated in Figure 2.

Most common multiobjective optimizers solve (1-2) by creating first an initial population $\mathbf{P}^{(0)} = \{\mathbf{p}_1^{(0)}, \dots, \mathbf{p}_{n_{\text{LHS}}}^{(0)}\}$, e.g., using Latin hypercube sampling (LHS) [12]. For each realization $\mathbf{p} \in \mathbf{P}^{(0)}$ a finite element approximation of a magneto-static problem, e.g. on a 2D parameterized geometry $\Omega(\mathbf{p}) \subset \mathbb{R}^2$

$$-\nabla \cdot (\nu \nabla A_z(\mathbf{p})) = J_{\text{src},z}(\mathbf{p}) + \nabla \times \mathbf{M}(\mathbf{p}) \cdot \mathbf{e}_z, \quad (3)$$

is required, [13], [14]. Here, the (nonlinear) reluctivity is denoted by ν , the z-component of the magnetic vector potential by $A_z(\mathbf{p})$, the current density by $J_{\text{src},z}(\mathbf{p}) = \sum_k \chi_k i_k(\mathbf{p})$ in terms of winding functions χ_k and currents $i_k(\mathbf{p})$ [15]. The magnetization of the permanent magnets is taken into account by $\mathbf{M}(\mathbf{p})$ and homogeneous Dirichlet boundary conditions $A_z = 0$ are set on $\partial\Omega$. The computed electromagnetic fields are post-processed with various cross-domain tools and the end-results of this analysis are the KPIs used for optimization. They will be addressed by

$$y_j^{(i)} := y_j(A_z(\mathbf{p}^{(i)}), \mathbf{p}^{(i)}). \quad (4)$$

The pareto front consisting of the current optimal designs is created from those evaluations. Then, the optimizer generates new ensembles $\mathbf{P}^{(i)}$ ($i > 0$) e.g. with an evolutionary algorithm by selecting, recombining, and mutating [16]. The process repeats until convergence, see Figure 2. The entire operation will take days or weeks depending on the availability of high performance computing resources. Meta-models which approximate the KPIs y_j by inexpensive surrogates \tilde{y}_j can overcome the computational burden by reducing the amount of evaluations of the costly FE problem (3).

B. META-MODEL

Meta-modelling imitates the behavior of computationally expensive simulation model to evaluate desired objective functions as close as possible to the actual with being computationally cheap. Polynomial interpolation (also known as spectral method or polynomial chaos) is often used, in particular in the context of uncertainty quantification [17]–[19]. On the other hand, Kriging is another common approach to obtain a meta-model under suitable assumptions on priors [20]. In order to solve the optimization problem of electromagnetics in an inexpensive way, the possibility of meta-modelling with Kriging is for example proposed in [21]. To optimize electromagnetic design by putting focus on achieving balance between exploitation and exploration

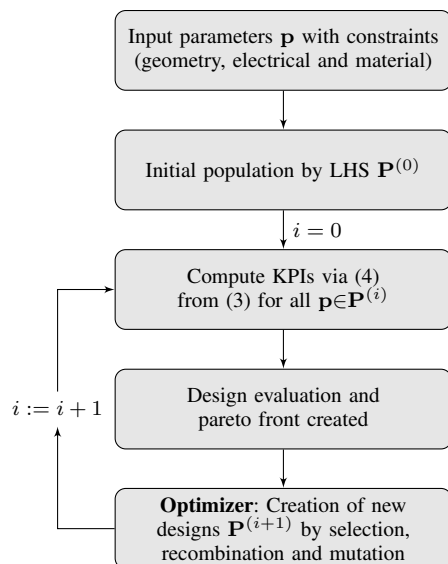


Figure 2: Flowchart of the process for calculating KPIs

during global optimum search with Kriging is proposed in [22]. It is demonstrated in [23], how Kriging can be combined with evolutionary algorithms for MOO of PMSM design to lower the time-consuming computations. In [24], to enhance sensorless control capability along with torque behavior of the multi-objective surface mounted PMSM design for decreased optimization calculation time, a Kriging supported evolutionary algorithm is proposed.

At present, fast-paced developments in the domain of machine learning (ML), especially with deep learning, have unfolded new insight for complex non-linear function approximation for multi-output regression [25], [26]. The convolutional neural network (CNN) which is a special class of artificial neural network has been used for decades now. The advantage of CNN is the extraction of features to represent the hierarchical expression of image form data [27] [28]. The applications of CNN in various fields increased after the success in the image net challenge (classification and object detection via supervised learning) [29]. The ability to transfer pre-trained network knowledge from one application to another makes it prominent for faster training. It has shown good results even when training data is limited [30].

In the domain of electrical machines, deep learning applications are still in an early stage. The prediction of efficiency, speed and torque using DL based multi-regression was demonstrated for the performance analysis of PMSMs in [31]. In [32] it is shown how hybrid electric vehicles at system level can be optimized by modeling non-linear system behavior using neural networks. In another article, estimation of the magnetic field solution for different EM devices such as a coil in air, a transformer, and an interior permanent magnet (IPM) machine have been investigated by using deep CNNs [33]. There is an application with recurrent neural network (RNN) and CNN for real time monitoring of high-fluctuating temperature inside PMSMs probed in [34]. Deep

neural networks were shown to work as torque predictors for different states of (steady or transient) interior PMSM drives [35]. DL based on CNN has been shown to be effective for quick evaluation of electric motor performance in order to reduce FE analysis for the topology optimization [36]. This idea has been expanded for multi-objective topology optimization using Deep convolutional neural network (DCNN) [37]. The efficiency map for a motor drive was computed with DL in [38]. One of the recent work demonstrates a multi-layer perceptron as a meta-model for shape optimization of PMSMs [39]. In the recent past, a combination of the CNN based model and a reduced FE model were analyzed for accelerated optimizations in electromagnetics [40].

C. COMPARISON OF PARAMETER AND IMAGE BASED META-MODELS

The image-based approach is a very general way to access the performance of the electrical machine. The DL based meta-model becomes deterministic, once it is trained. The image-based DCNN model only considers the final image space in which it was trained. It is not concerned with how it is generated. So if we re-parameterize such that image space remains invariant, then it is possible to predict the KPIs by the same image based trained meta-model. However, this does not hold for (scalar) parameter based meta-models as any re-parametrization alters the input space. For example, as shown in Figure 3, two plates are differently parameterized but have the same image space. The plate 1 is generated with input scalar parameters a, b while plate 2 is produced with parameters d, e which are different. Now, if we train a parameter based meta-model with the input space of parameters a, b and test with input space of parameters d, e to make predictions, e.g. about the stiffness of plate, then it will not give correct prediction (if we do not find a suitable transformation). On the contrary, an image based trained DCNN model will still give correct predictions.

III. DATASET GENERATION

In this study, an optimization workflow is applied to generate a large amount of training data. Two datasets are considered. Each set consists of machine realizations, i.e., the parameter values $\mathbf{p}^{(i)}$, the Computer-Aided Design (CAD) models, which are then used for simulation and the corresponding KPIs $y_j^{(i)}$. Details on two datasets can be found in the following subsections. Only a half pole and full pole cross-section are considered in both datasets since geometrical symmetry of the electrical machines can be exploited.

A. DATASET 1

The rotor model takes into account $n_p = 49$ scalar parameters for the generation of samples. Seven important stator parameters that represent stator geometry information are detailed in Table 1. Other electrical parameters such as the number of slots, phase current, phase voltage, which remain constant during the data generation are given in Table 2. Likewise, material features such as copper filling factor,

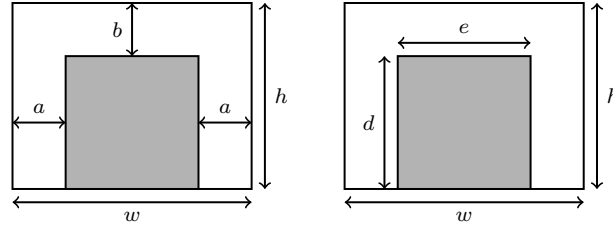


Figure 3: Differently parameterized plates with the same image space ($e = w - 2a$ and $d = h - b$)

Table 1: Stator parameter detail dataset 1

	Parameter	Min.	Max.	Unit
p_1	Tooth head overhang 1	0.76	1.19	mm
p_2	Height of tooth head	12.41	18.91	mm
p_3	Tangential groove width	4.23	6.37	mm
p_4	Stator inner diameter	143.41	158.34	mm
p_5	Tooth head overhang 2	1.20	1.64	mm
p_6	Tooth width near air gap	5.05	8.60	mm
p_7	Iron length	160.49	168.00	mm

Table 2: Constant parameters

Parameter	Dataset 1	Dataset 2	Unit
No pf pole pair	4	4	-
Stator type	Asymmetric	Asymmetric	-
Rotor type	VC-Design	VC-Design	-
No of slots (stator)	48	48	-
Max. phase voltage	640	640	V
Max. phase current	480	600	A
Slots per pole per phase	2	2	-

Table 3: KPIs information dataset 1

	KPI	Unit
y_1	Costs of active parts	Euro
y_2	Critical field strength,	kA/m
y_3	Maximum torque of machine	Nm
y_4	Maximum power of machine	W
y_5	Weighted efficiency value	%
y_6	Maximum torque-ripple	Nmp
y_7	Torque-ripple behavior of machine	-
y_8	Inverter losses	W
y_9	Sound power level of machine	dBA
y_{10}	Maximum magnet temperature	K
y_{11}	Maximum winding temperature	K

remanence, and type of magnet cluster also remain invariant. The Table 3 gives a short description of the KPIs. The distributions in the spaces of parameters and KPIs of the model and its simulation results are visualized on affine 2D subspaces in Figure 4a and Figure 4c, respectively. The total number of samples produced using the Figure 2 process is $n_1 = 68099$ and the distribution of the input parameters is rather inhomogeneously distributed.

The pre-processing of the data involves the transformation of the parameterized CAD model into a rectangular pixelized image in which each pixel has a unique identifier value related to the electrical machine component (air: 0, metal: 1, magnet: 2). The resulting cross-sectional images of a half pole of the rotors, shown for one example in Figure 5, are used for the images-based training.

One interesting observation is that the parameter-based KPI estimation is only depends on the scalar parameters such that a even a tiny change of a single parameter will in general lead to a different prediction while the image-based model relies on the image accuracy. In an initial examination, a resolution of 136×216 pixels for the geometrical domain $79\text{mm} \times 50\text{mm}$ is selected. This results in 0.36mm/pixel which is larger than the minimum variation of any input scalar parameter, in other words, it takes approx. 3 pixels

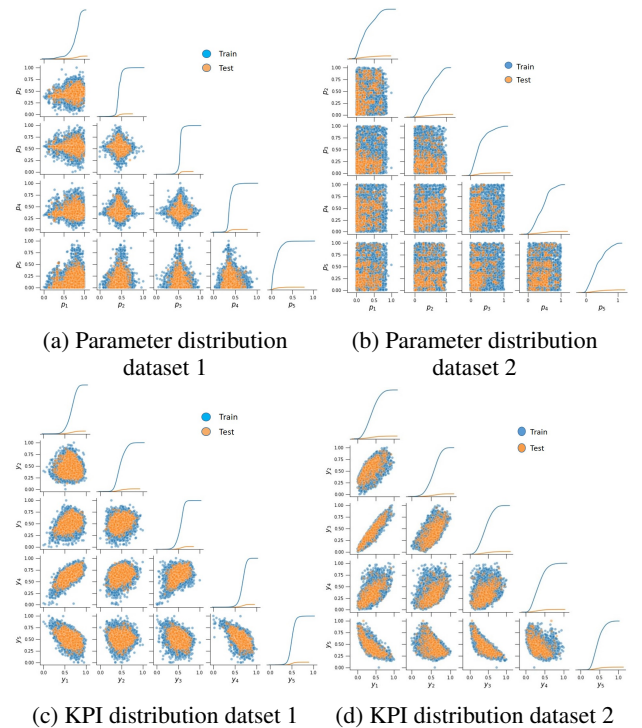


Figure 4: Parameter and KPI distributions

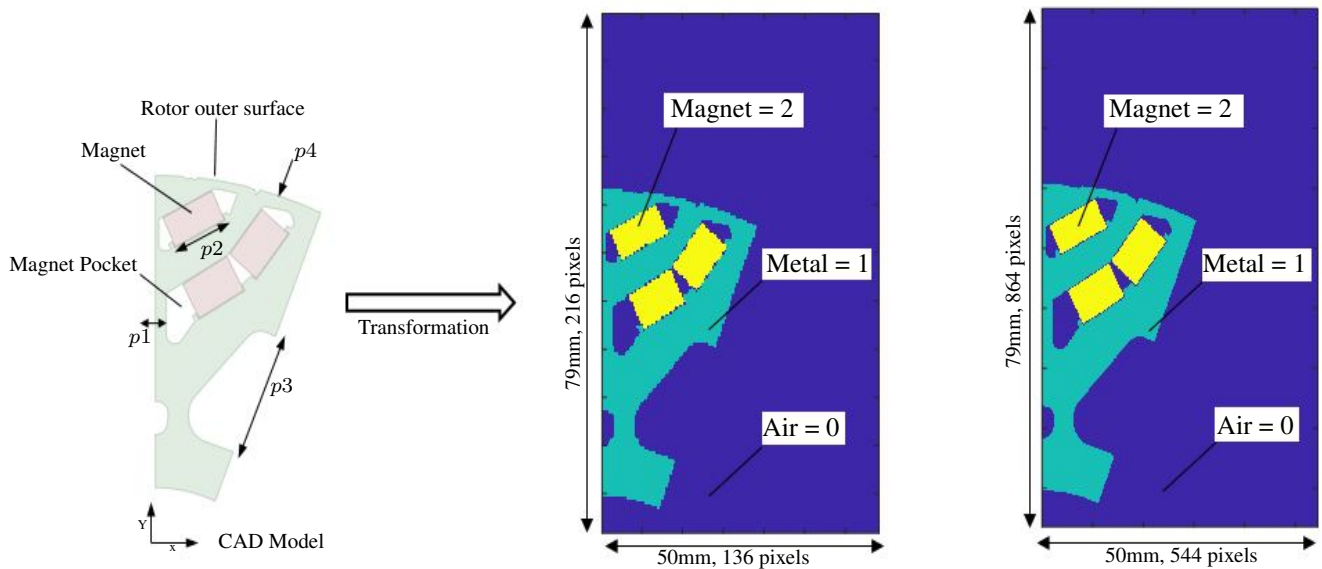


Figure 5: Dataset 1 visualization

Table 4: Pixel Resolution Detail concerning to geometry parameter variation with dataset 1

	Min [mm]	Max [mm]	Image resolution in pixels, X-direction=50mm, Y-direction=79mm					
			Precision [mm/pixel]			Pixel value		
			136 × 216	272 × 432	544 × 864	136 × 216	272 × 432	544 × 864
p_1	0.8528	1.4895	0.3676	0.1838	0.0919	2	4	7
p_2	7.1938	9.4859	0.3676	0.1838	0.0919	7	13	26
p_3	6.6480	12.967	0.3676	0.1838	0.0919	18	35	70
p_4	141.6990	155.3637	0.3676	0.1838	0.0919	38	75	149

to indicate a change of 1mm in a geometry parameter. This obviously affects the sensitivity of the network. Thus, if the pixel precision is increased, the interpretation of variations in the geometry parameters is enhanced. Four rotor parameters, which vary from minimum to maximum range, are set out in Table 4. The last three columns in the table give data about how many number of pixels required to show variation in the geometry for a unit length. Eventually, we compare three resolution values, 136×216 , 272×432 and 544×864 pixels.

B. DATASET 2

Figure 6 illustrates dataset 2. It differs from dataset 1 by its parametrization, which is now given in terms of $n_p = 12$ values, and consequently by the image form. In the geometry image the stator and the rotor full pole cross-sections are visible. The transformed pixel-matrix includes an additional identifier tag value 3 to show copper material. Twelve major variable scalar parameters (rotor and stator) with their respective ranges are specified in Table 6. Other constant parameters similar to dataset 1 appear in Table 2. Table 5 details the respective KPIs. In the Figure 4d and Figure 4b respectively, the joint distribution of KPIs and scalar parameters is shown. The distribution of input parameters is almost uniform. For this dataset, the total number of samples

Table 5: KPIs information dataset 2

	KPI	Unit
y_1	Total cost	€
y_2	Maximum torque of machine	Nm
y_3	Maximum power at maximum rpm	KW
y_4	Iron losses	W
y_5	Copper losses	W
y_6	Maximum torque ripple	Nmp
y_7	Mass of iron	Kg
y_8	Mass of copper	Kg
y_9	Mass of magnet	Kg
y_{10}	Torque-ripple behavior of machine	-

generated is $n_2 = 7744$

IV. NETWORK ARCHITECTURE AND TRAINING

The network architecture is being determined based on the form of input data used for the training. A deep neural network (DNN) or multilayer perceptron (MLP) architecture is derived for the meta-model based on scalar parameters. The DCNN is used for image-based data training. The network structure of Figure 11 is also applied for the input combination of scalar and image-based data. The idea here is to explore how different forms of input data can affect

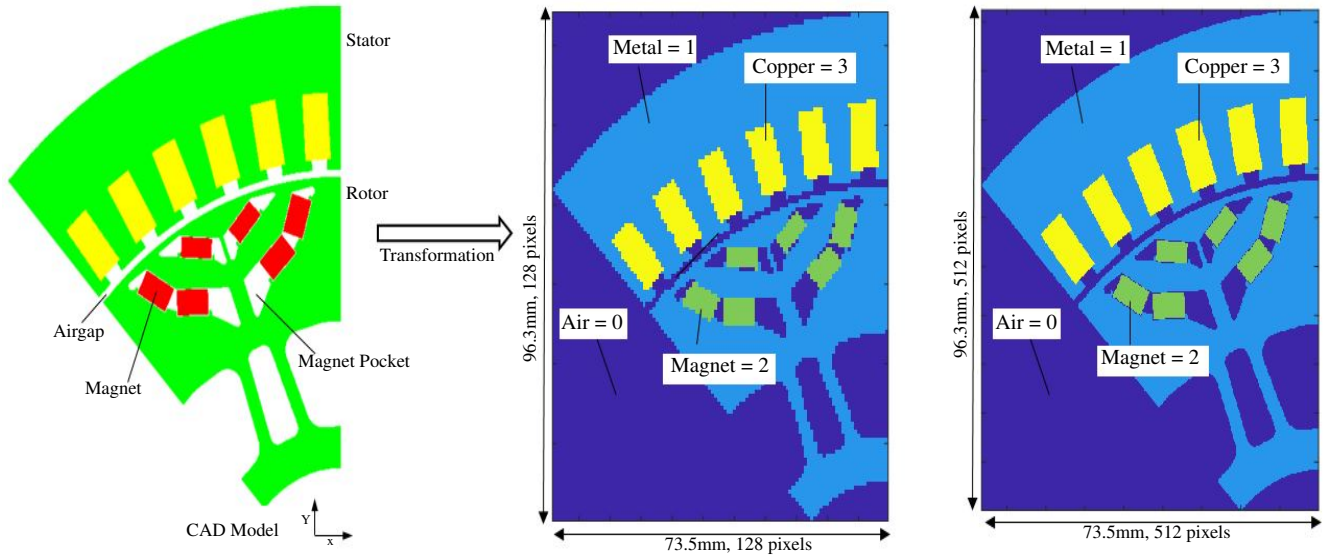


Figure 6: Dataset 2 visualization

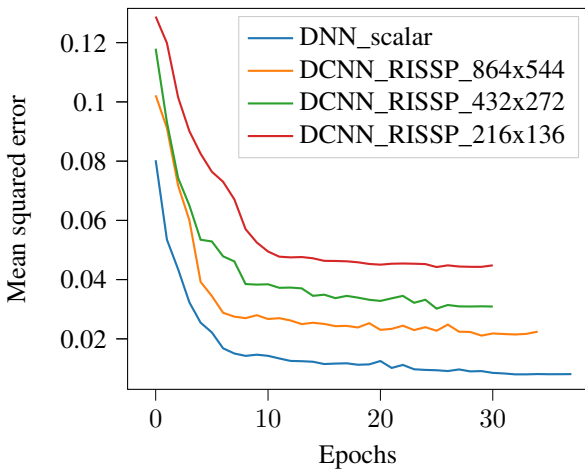


Figure 7: Training curve over validation set (Dataset 1). RISSP is short for rotor image and stator scalar parameters.

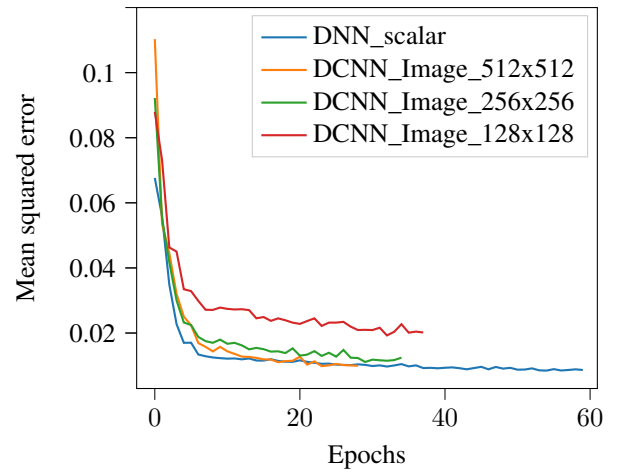


Figure 8: Training curve over validation set (Dataset 2)

Table 6: Parameter detail dataset 2

	Parameter	Min.	Max.	Unit
p_1	Angle of inner magnets	15	40	degree
p_2	Height of outer magnet	3	7	mm
p_3	Pole angle of outer magnet	45	80	degree
p_4	Height of tooth head	4	7	mm
p_5	Rotor outer diameter	160	170	mm
p_6	Height of inner magnets	4	7	mm
p_7	Width of inner magnets	7.0	11.5	mm
p_8	Angle of inner magnets	28	58	degree
p_9	Width of outer magnet	7	12	mm
p_{10}	Angle of outer magnet	15	38	degree
p_{11}	Height of tooth head	12	17	mm
p_{12}	Tooth head width	5	9	mm

predictive accuracy. The scalar parameters contain the full information of both rotor and the stator. While the combination of half-pole rotor cross-section image and stator parameters for dataset 1 sets the visual and scalar information of the electrical machine model. The images consist only of geometric details for the rotor and stator cross-sections for dataset 2. A trial and error approach was used to finalize three different candidates for each input. Details on the network architecture for each of these inputs are provided in the following subsections.

A. DNN STRUCTURE

The MLP based DL model is shown in Figure 9 comprises of five dense layers. The network has an input layer with number of scalar parameters (rotor, stator) and output layer

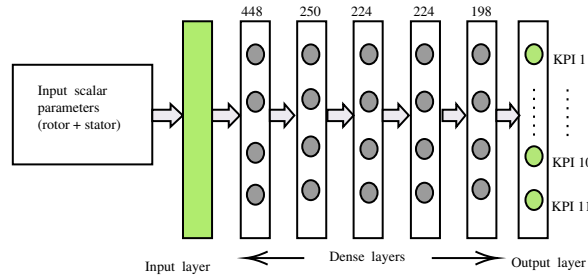


Figure 9: DNN: scalar parameter based meta-model

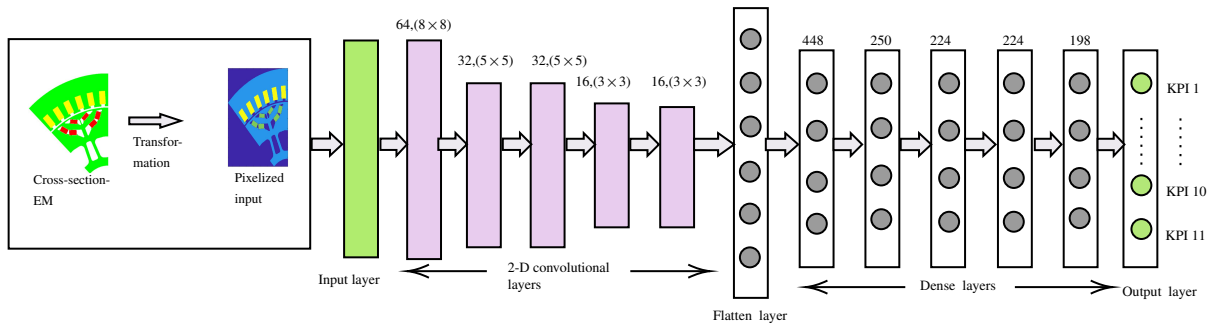


Figure 10: DCNN: image based meta-model

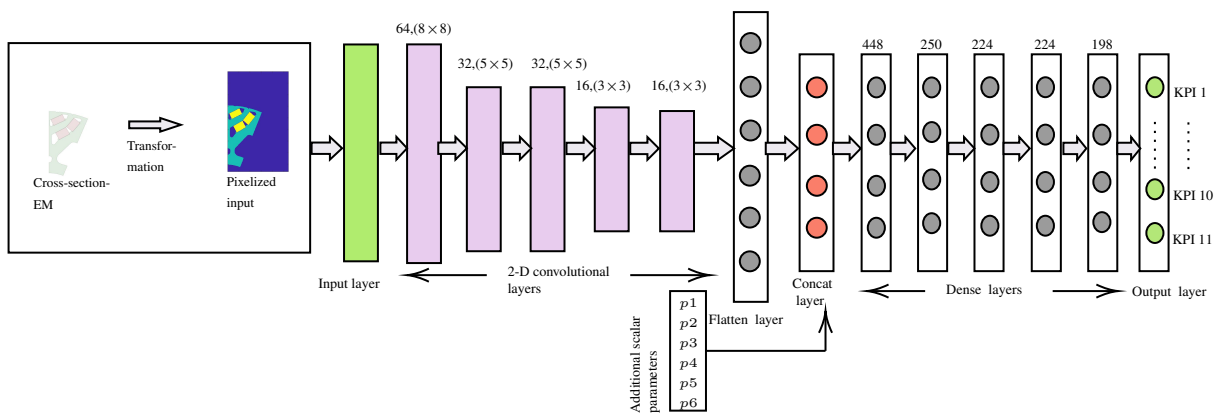


Figure 11: DCNN with additional scalar input

neurons with the number of target KPIs. The whole structure is defined as $56 - 448 - 250 - 224 - 224 - 198 - 11$ and $12 - 448 - 250 - 224 - 224 - 198 - 10$ for dataset 1 and dataset 2, respectively. The ELU activation function has been chosen from the different non-linear activation functions between hidden layers [41].

B. DCNN STRUCTURE

The network architecture, as indicated in Figure 10, consists of two parts: convolution layers and dense layers. The objective of the convolutional layers is to extract spatially related features from the visual form of the input geometry. The dense layer section then uses this information to semantically project the discriminatory features that the convolution layers have extracted to predict KPIs in the final output layer. It must have sufficient capacity to successfully capture the

complexity of the problem to train the network effectively. This functionality is accomplished by selecting an experience value by trial and error for the number of layers, the number of kernels(64, 32, 16), the kernel size(8×8 , 5×5 , 3×3), and regularization parameters(learning rate). As presented in Figure 10, there are five convolutional layers for down sampling. This network architecture is invariant to the input dimension. The dense layer structure after flattening the layer is the same as the model based on scalar parameters, see Figure 9, to allow for reasonable comparisons.

C. MULTI-INPUT DCNN STRUCTURE

The network architecture remains the same in this model as in the preceding subsection IV-B. The only difference being that the additional input layer is concatenated with the output of the convolution layer as shown in Figure 11. Detailed in-

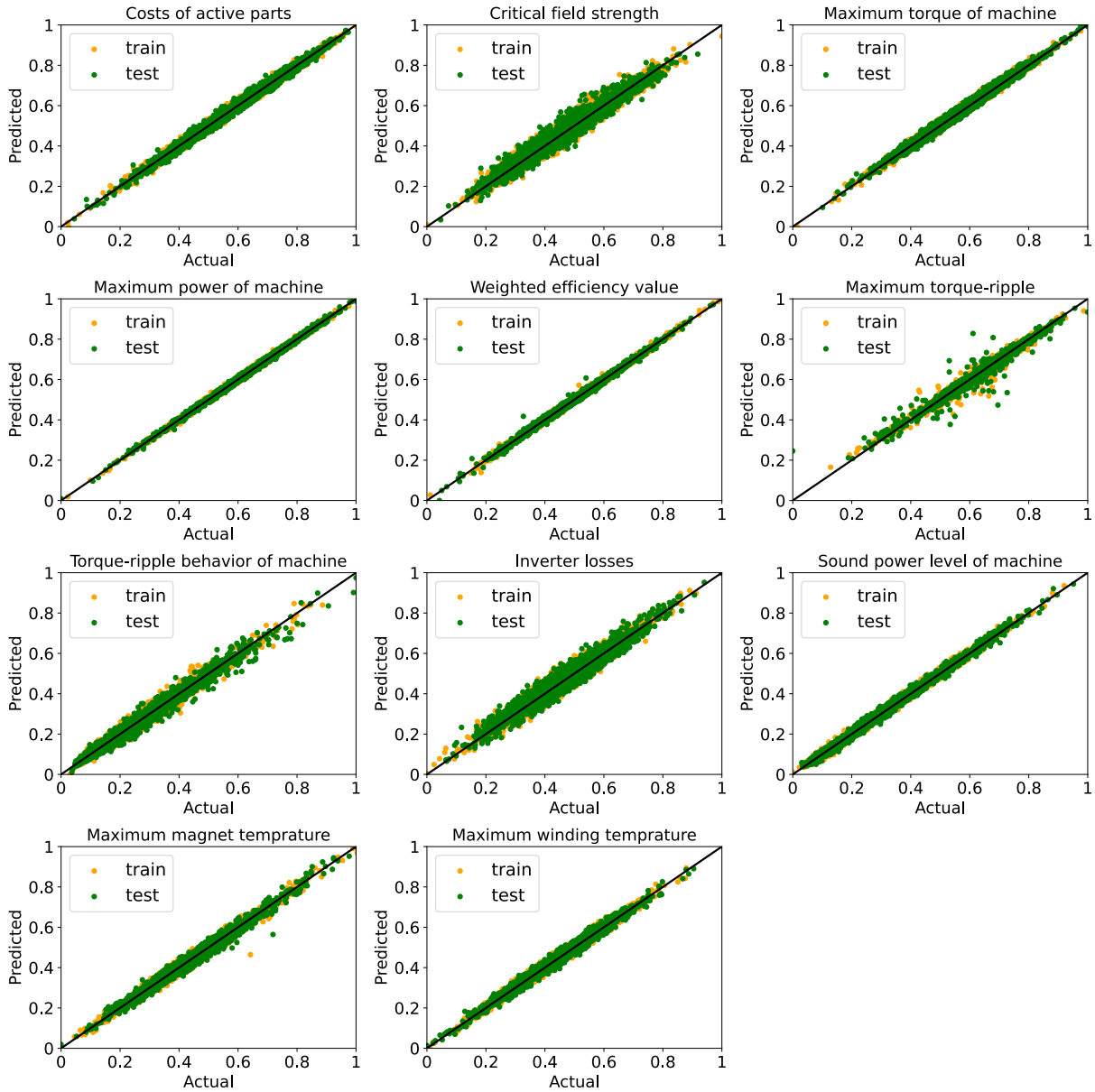


Figure 12: KPI prediction dataset 1 with scalar based meta-model

formation is provided in Table 1 for various scalar parameters of the stator geometry for dataset 1. The reason for this is to provide information on the missing stator geometry. This multi-input structure is only used for dataset 1 training as dataset 2 has already stator geometry information in image form.

D. TRAINING PROCESS

The data set is partitioned into training, validation and test sets. The networks are trained on the training set with back-propagation algorithm [42] to learn any arbitrary mapping of input parameters to output KPIs. Hyper-parameters include the total number of training epochs maximum (100), batch size (50), early stopping over validation error(not decreasing continuously for 5 epochs compared to the lowest error

recorded so far during training), learning rate range (0.001-0.0001), metric evaluation (mean squared error), non-linear activation function (ELU), and optimizer (Adam) [43], network depth (count of hidden layers), and number of hidden units within each layer. Hyper-parameters also play a role in the model’s performance to an extent, but it is difficult to fix specific values, so they are chosen randomly (trial and error) and kept constant for all the three model candidates to be trained. As mentioned in the sectionIII, dataset 1 and dataset 2 consists of $n_1 = 68099$ and $n_2 = 7744$ samples, respectively. Approximately 90% of the total number of samples is used during the training process, while around 5% is reserved for validation and testing of both datasets, i.e.,for dataset 1: $n_{train} = 61290$, $n_{validation} = 3405$, $n_{test} = 3404$ and for dataset 2 $n_{train} = 6970$, $n_{validation} = 387$, $n_{test} =$

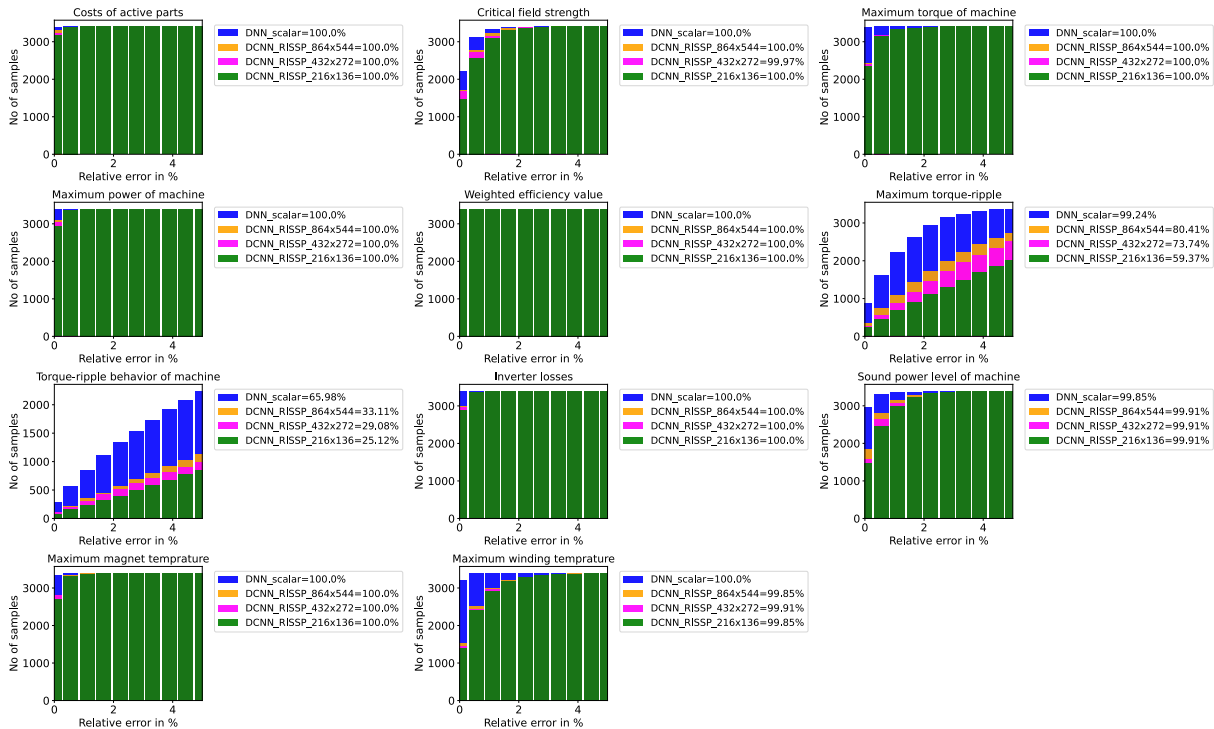


Figure 13: Cumulative accuracy plots of the KPI prediction with relative error $\epsilon_{mre} < 5\%$ dataset 1

387. Figure 7 and Figure 8 shows training curve over the validation set for all the meta-models. The entire training process is carried out on a NVIDIA Quadro M4000 GPU. All the deep learning-based meta-models implemented using numerical computational library TensorFlow [44]. Training on the scalar parameter based MLP model takes approximately 1 minute to 4 minutes for the dataset 2 and dataset 1 respectively. For the training of image based DCNN models, roughly 1 to 8 minutes per epoch (depending on image resolution, total number of training samples, and batch size), resulting in a total run time of 1 h to 6 h for both datasets. All meta-models take about ~ 1 ms/sample to evaluate new geometries that is much lower than the FE model, which calculates 6 h to 8 h on a single core CPU for one evaluation. If memory requirements are met, the advantage of parallelization over GPU during the training process can be further utilized with a higher number of geometries. The meta-model can then be trained in a short time, and thus the duration of training is memory-bound rather than compute-bound[33]. Therefore, training time is greater for the large dataset(dataset 1).

V. RESULTS AND ANALYSIS

As the problem characterizes as a non-linear multi-output regression and all the KPIs are on different scales, the dimensionless mean relative error (MRE), [45], i.e.,

$$\epsilon_{mre}(y_j) = \frac{1}{n_{test}} \sum_{i=1}^{n_{test}} \frac{|y_j^{(i)} - \tilde{y}_j^{(i)}|}{|y_j^{(i)}|} \times 100 \quad (5)$$

is selected for the final evaluation of the j -th KPI on the n_{test} -dimensional validation data set. It quantifies how accurate the prediction $\tilde{y}_j^{(i)}$ is compared to the true value $y_j^{(i)}$ for a given parameter configuration $\mathbf{p}^{(i)}$. On the other hand the Pearson correlation coefficient (PCC)

$$\epsilon_{pcc}(y_j, \tilde{y}_j) = \frac{\sum_{i=1}^{n_{test}} (y_j^{(i)} - \bar{y}_j^{(i)})(\tilde{y}_j^{(i)} - \bar{\tilde{y}}_j^{(i)})}{\sqrt{\sum_{i=1}^{n_{test}} (y_j^{(i)} - \bar{y}_j^{(i)})^2} \sqrt{\sum_{i=1}^{n_{test}} (\tilde{y}_j^{(i)} - \bar{\tilde{y}}_j^{(i)})^2}} \quad (6)$$

gives an idea of how the input parameters are mapped to the target output values [46]. If the PCC is close to one between the predicted and the actual values, then the performance of the model is better.

A. EVALUATION OF DATASET 1

Figure 12 displays the predicted KPIs for the dataset 1 over their actual target values. An evaluation of all the KPIs is presented in Table 7 over their mean values. A cumulative plot for below 5% relative error is shown Figure 13. The MLP based model has input information on geometry parameters from both, the stator and the rotor, while the deep multi-input network Figure 11 receives information in form of the half-pole rotor cross-section image and the stator geometry configuration. Training, test, validation set and hyper parameter settings remains constant during the training of all the meta-models.

The KPIs related to the torque behavior of the machine, e.g., y_6, y_7 , have lower prediction performance compared to other KPIs with average ϵ_{mre} i.e., ϵ_{mre} 4.22% and 1.28%, respectively, see Table 7. It can be observed that the average

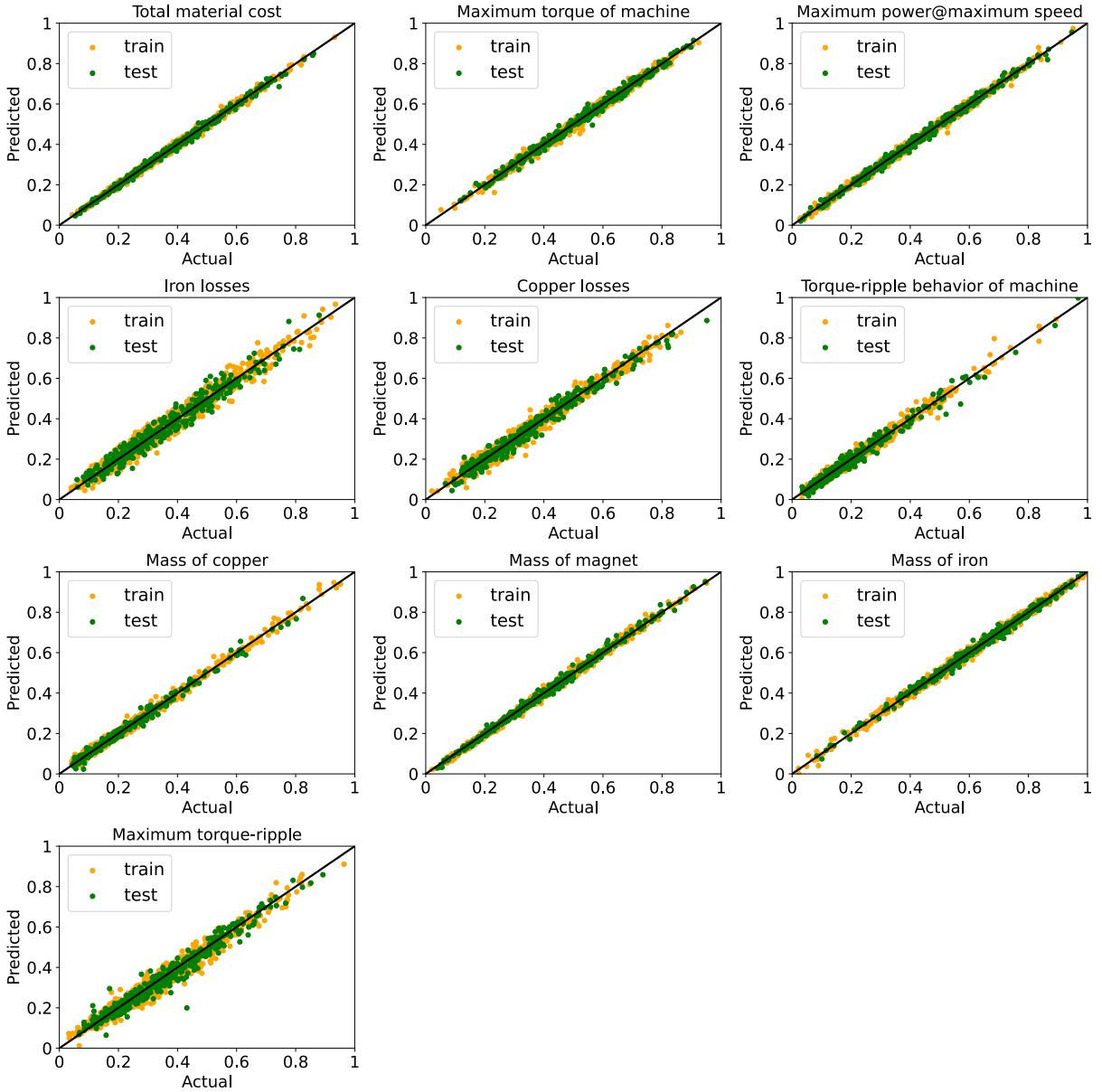


Figure 14: KPI prediction dataset 2 with scalar based meta-model

ε_{mre} over all the KPIs for the DNN is 0.64% which is much lower than the best performing multi-input DCNN model (with resolution 544×864 pixel) with average ε_{mre} of 1.43%. The DCNN based multi-input meta-model is trained and evaluated with three different image resolutions. The network architecture is shown in Figure 11. The network with the higher resolution image data (864×544) has average ε_{mre} 1.43% over all the KPIs that is $\sim 12.05\%$ and $\sim 24.96\%$ lower than the input data with image resolution 432×272 and 216×136 , respectively. Detailed result is described in Table 7. However, as a consequence of the higher resolution, the network takes twice or sometimes even more time to train as compared the lower one, i.e., approx. 1h (136×216 pixel) vs. approx. 2h (272×472 pixel) with average over all KPIs ε_{mre} lower $\sim 14.68\%$ for high resolution, so it is trade-off

between the training time of meta-model and performance.

B. EVALUATION OF DATASET 2

Dataset 2 has fewer samples which are more uniformly distributed than dataset 1 and has a different set of KPIs as well. Prediction plot and evaluations are exhibited in Figure 14 and Table 8, respectively. A cumulative plot for the error is illustrated in Figure 15. The KPIs related to the machine torque (y_6 and y_{10}) have the down predicatibility than other KPIs with average ε_{mre} 5.9% and 3.47% over all the KPIs. It is also evident from the results that the prediction accuracy improves with image accuracy for this dataset, too. The scalar parameter based meta-model has average ε_{mre} 1.66% which is 7.45%, 15.78%, 34.28% lower than the image based DCNN 512×512 , image based DCNN 256×256 , and 128×128 ,

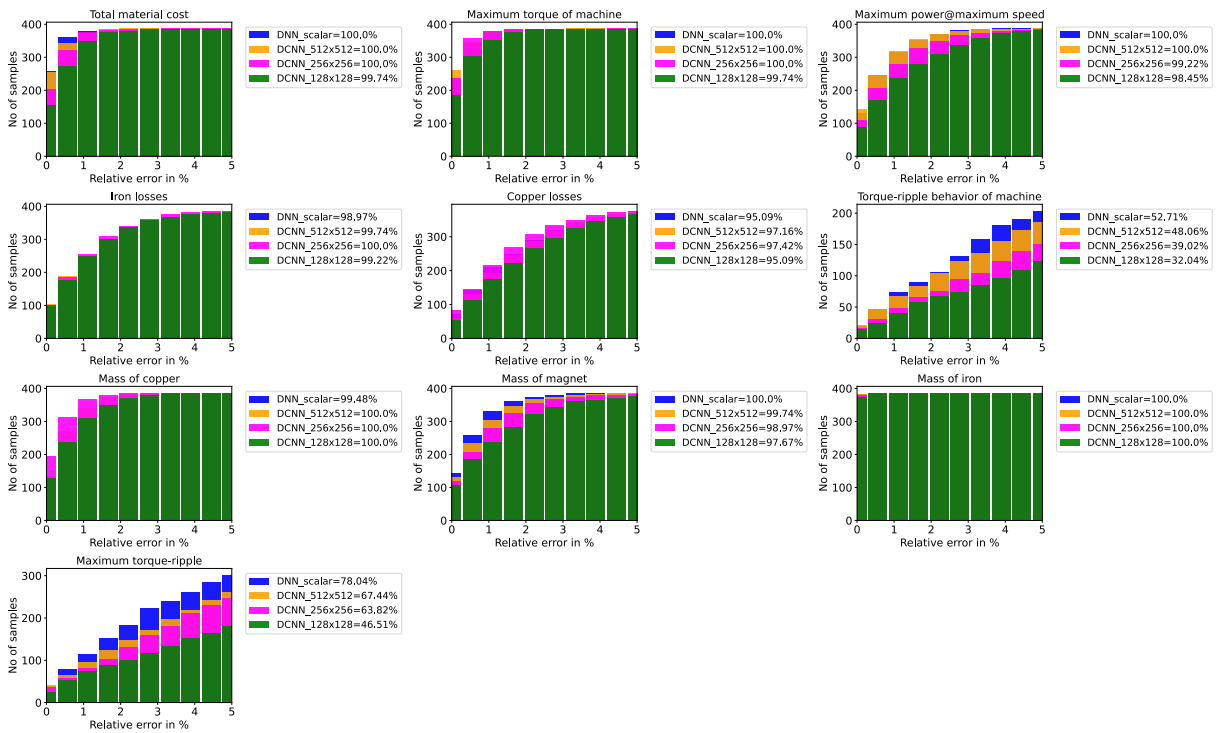


Figure 15: Cumulative accuracy plots of the KPI prediction with relative error $\epsilon_{mre} < 5\%$ dataset 2

Table 7: Evaluation summary dataset 1

	DNN		DCNN 544 × 864		DCNN 272 × 432		DCNN 136 × 216	
	ϵ_{mre}	ϵ_{pcc}	ϵ_{mre}	ϵ_{pcc}	ϵ_{mre}	ϵ_{pcc}	ϵ_{mre}	ϵ_{pcc}
y_1	0.12	0.99	0.17	0.99	0.20	0.99	0.22	0.98
y_2	0.44	0.97	0.60	0.96	0.64	0.97	0.70	0.95
y_3	0.12	0.99	0.41	0.98	0.42	0.93	0.42	0.93
y_4	0.05	0.98	0.24	0.98	0.25	0.95	0.27	0.94
y_5	0.01	0.94	0.05	0.92	0.05	0.90	0.06	0.89
y_6	1.28	0.98	2.99	0.97	3.55	0.96	4.77	0.95
y_7	4.22	0.95	9.4	0.94	10.69	0.92	12.34	0.89
y_8	0.13	0.98	0.26	0.98	0.26	0.98	0.28	0.96
y_9	0.29	0.96	0.55	0.95	0.71	0.94	0.76	0.94
y_{10}	0.16	0.98	0.32	0.94	0.35	0.93	0.35	0.91
y_{11}	0.21	0.96	0.76	0.95	0.79	0.95	0.82	0.95

Table 8: Evaluation summary dataset 2

	DNN		DCNN 512 × 512		DCNN 256 × 256		DCNN 128 × 128	
	ϵ_{mre}	ϵ_{pcc}	ϵ_{mre}	ϵ_{pcc}	ϵ_{mre}	ϵ_{pcc}	ϵ_{mre}	ϵ_{pcc}
y_1	0.42	1.00	0.47	1.00	0.56	1.00	0.78	0.99
y_2	0.51	1.00	0.45	1.00	0.46	0.99	0.68	0.98
y_3	0.91	1.00	0.90	1.00	1.16	0.99	1.49	0.99
y_4	1.52	0.98	1.33	0.99	1.26	0.99	1.31	0.96
y_5	1.83	0.99	1.82	0.99	1.64	0.99	2.06	0.97
y_6	5.9	0.98	6.70	0.98	7.99	0.96	9.67	0.97
y_7	1.06	0.99	0.78	0.99	0.62	0.98	0.93	0.94
y_8	0.84	1.00	0.97	1.00	1.15	1.00	1.53	0.98
y_9	0.13	1.00	0.14	1.00	0.14	1.00	0.17	0.99
y_{10}	3.47	0.98	4.36	0.98	4.72	0.97	6.58	0.95

respectively. Here, it is important to note that dataset 2 has a less scalar parameters, i.e., 12 and cross-section of EM consists geometry information of one full pole rotor and stator.

C. DNN AND GAUSSIAN PROCESS REGRESSION FOR PARAMETER BASED META-MODELS

This work focuses on meta-modeling approaches based on deep learning as they promise to efficiently treat image based data [29]. However, to allow for a comparison with other state of the art approaches, also Kriging, or more precisely, Gaussian process regression (GPR, see e.g. [47]), is applied in the case of parameter based learning. The GPR meta-model is trained using the sci-kit-learn library [48], [49] with its default settings, i.e., radial-basis function kernel (RBF 1.0)

and default optimizer L-BGFS-B [50], [51]. The RBF kernel is often used in practice, however, a more rigorous quantitative comparison should take other kernels into account but this is beyond the scope of this paper. For dataset 1, all the KPIs have similar performance except torque related KPIs for which the DNN-based meta-model has around 50% less error than the GPR based meta-model. Figure 16 illustrates the outcomes of both approaches concerning dataset 2. The results show that the DNN-based meta-model for all the KPIs clearly outperforms the GPR-based meta-model. The training time for the GPR based meta-model is approx. 10 times larger than for the DNN. Dataset 1 has a large number of samples and higher dimensional input space compared to dataset 2, therefore the GPR-based meta-model was trained in two separate runs due to memory constraints.

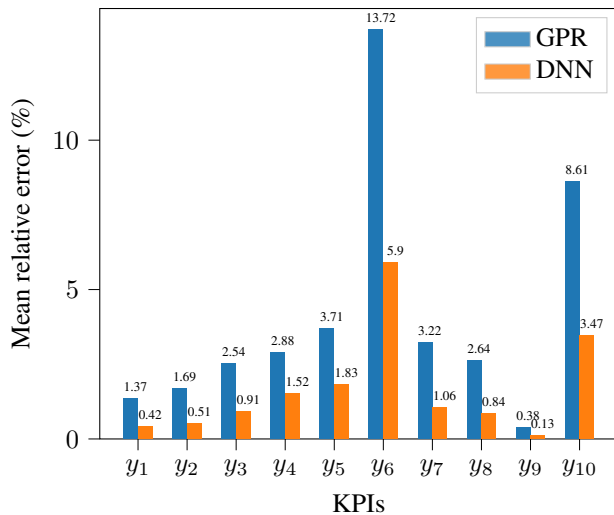


Figure 16: Dataset 2 : KPIs performance comparison for parameter based meta-model

VI. CONCLUSION

This contribution shows that the deep learning meta-models can be effectively used to approximate a large number cross-domain KPIs in a high dimensional parameter space. The data for demonstration is taken from a real-world industrial design workflow. The meta-model enables us to predict KPIs for new geometries at much lower computational costs. The prediction performance depends on how accurately the input information can be mapped to the target KPIs. The mapping accuracy relies mainly on two factors, hyper-parameter settings and the precision of the input data. In this work, hyper-parameter settings are the same for all meta-models and the focus is on the precision of the input data. This paper proposes two models for parameter and image-based learning. The image-based approach increases the flexibility and re-usability of the model for example in the case of a reparametrization. Our results show that it performs close to scalar-parameter-based models if the pixel resolution of the training data is sufficient. Future work will make use of the meta-model in many-query-scenarios, e.g., uncertainty quantification or multi-objective optimization.

References

- [1] M. Kondo, J. Kawamura, and N. Terauchi, "Performance comparison between a permanent magnet synchronous motor and an induction motor as a traction motor for high speed train," *IEEE Transactions on Industry Applications*, vol. 126, no. 2, pp. 168–173, Jan. 2006. DOI: 10.1541/ieejias.126.168.
- [2] K. T. Chau, C. C. Chan, and C. Liu, "Overview of permanent-magnet brushless drives for electric and hybrid electric vehicles," *IEEE Transactions on Industrial Electronics*, vol. 55, no. 6, pp. 2246–2257, 2008. DOI: 10.1109/TIE.2008.918403.
- [3] G. Pellegrino, A. Vagati, B. Boazzo, and P. Guglielmi, "Comparison of induction and pm synchronous motor drives for ev application including design examples," *IEEE Transactions on Industry Applications*, vol. 48, no. 6, pp. 2322–2332, 2012. DOI: 10.1109/TIA.2012.2227092.
- [4] Y. Duan and D. M. Ionel, "A review of recent developments in electrical machine design optimization methods with a permanent-magnet synchronous motor benchmark study," *IEEE Transactions on Industry Applications*, vol. 49, no. 3, pp. 1268–1275, 2013. DOI: 10.1109/TIA.2013.2252597.
- [5] M. Rosu, P. Zhou, D. Lin, D. M. Ionel, M. Popescu, F. Blaabjerg, V. Rallabandi, and D. Staton, *Multiphysics Simulation by Design for Electrical Machines, Power Electronics and Drives*. Wiley-IEEE Press, Dec. 2017, ISBN: 978-1-119-10344-8.
- [6] G. Bramerdorfer, J. A. Tapia, J. J. Pyrhönen, and A. Cavagnino, "Modern electrical machine design optimization: Techniques, trends, and best practices," *IEEE Transactions on Industrial Electronics*, vol. 65, no. 10, pp. 7672–7684, 2018. DOI: 10.1109/TIE.2018.2801805.
- [7] M. Ehrgott, *Multicriteria Optimization*. Springer, 2005, ISBN: 3-540-21398-8.
- [8] P. Di Barba, *Multiobjective Shape Design in Electricity and Magnetism*, ser. Lecture Notes in Electrical Engineering. Springer, 2010.
- [9] G. Lei, J. Zhu, Y. Guo, C. Liu, and B. Ma, "A review of design optimization methods for electrical machines," *Energies*, vol. 10, no. 12, p. 1962, 2017. DOI: 10.3390/en10121962.
- [10] Z. Tan and X. Gao, "A review of state-of-the-art control and optimization methods in permanent magnet synchronous machine drives," in *17th IEEE International Conference on Industrial Informatics (INDIN 2019)*, vol. 1, 2019, pp. 611–616. DOI: 10.1109/INDIN41052.2019.8972257.
- [11] G. Lei, G. Bramerdorfer, B. Ma, Y. Guo, and J. Zhu, "Robust design optimization of electrical machines: Multi-objective approach," *IEEE Transactions on Energy Conversion*, pp. 1–1, 2020. DOI: 10.1109/TEC.2020.3003050.
- [12] M. McKay, R. Beckkman, and W. Conover, "Comparison of three methods for selecting values of input variables in the analysis of output from a computer code," *Technometrics*, vol. 21, pp. 266–294, Jan. 2000. DOI: 10.1080/00401706.2000.10485979.
- [13] S. J. Salon, *Finite Element Analysis of Electrical Machines*. Kluwer, 1995.
- [14] M. Merkel, P. Gangl, and S. Schöps, "Shape optimization of rotating electric machines using isogeometric analysis," Cornell University, Preprint arxiv:1908.06009, Aug. 2019.
- [15] S. Schöps, H. De Gersem, and T. Weiland, "Winding functions in transient magnetoquasistatic field-

- circuit coupled simulations,” *COMPEL: The International Journal for Computation and Mathematics in Electrical and Electronic Engineering*, vol. 32, no. 6, pp. 2063–2083, Sep. 2013. DOI: 10.1108/COMPEL-01-2013-0004.
- [16] K. Deb, *Multiobjective Optimization Using Evolutionary Algorithms*. Wiley, 2001.
- [17] D. Xiu, *Numerical Methods for Stochastic Computations: A Spectral Method Approach*. Princeton University Press, 2010, ISBN: 978-0-691-14212-8.
- [18] S. Clénet, “Uncertainty quantification in computational electromagnetics: The stochastic approach,” *International Compumag Society Newsletter*, vol. 13, pp. 3–13, Mar. 2013, ISSN: 1026-0854.
- [19] Z. Bontinck, H. De Gersem, and S. Schöps, “Response surface models for the uncertainty quantification of eccentric permanent magnet synchronous machines,” *IEEE Transactions on Magnetics*, vol. 52, no. 3, Mar. 15, 2016, Article #7203404, ISSN: 0018-9464. DOI: 10.1109/TMAG.2015.2491607.
- [20] A. Forrester, A. Sobester, and A. Keane, *Engineering design via surrogate modelling: a practical guide*. John Wiley & Sons, 2008.
- [21] J. Sykulski, “New trends in optimization in electromagnetics,” in *2008 IET 7th International Conference on Computation in Electromagnetics*, 2008, pp. 44–49. DOI: 10.1049/cp:20080215.
- [22] S. Xiao, R. Mihai, and J. Sykulski, “Exploration versus exploitation using kriging surrogate modelling in electromagnetic design,” *COMPEL: The International Journal for Computation and Mathematics in Electrical and Electronic Engineering*, vol. 31, pp. 1541–1551, Sep. 2012. DOI: 10.1108/03321641211248291.
- [23] F. Bittner and I. Hahn, “Kriging-assisted multi-objective particle swarm optimization of permanent magnet synchronous machine for hybrid and electric cars,” in *2013 International Electric Machines Drives Conference*, 2013, pp. 15–22. DOI: 10.1109/IEMDC.2013.6556123.
- [24] M. Li, F. Gabriel, M. Alkadri, and D. Lowther, “Kriging-assisted multi-objective design of permanent magnet motor for position sensorless control,” *IEEE Transactions on Magnetics*, vol. 52, no. 3, pp. 1–4, 2016. DOI: 10.1109/TMAG.2015.2491301.
- [25] K. Hornik, M. Stinchcombe, and H. White, “Multi-layer feedforward networks are universal approximators,” *Neural Networks*, vol. 2, no. 5, pp. 359–366, 1989, ISSN: 0893-6080. DOI: 10.1016/0893-6080(89)90020-8.
- [26] S. Liang and R. Srikant, “Why deep neural networks for function approximation,” in *International Conference on Learning Representations (ICLR 2017)*, 2016.
- [27] Y. Lecun, L. Bottou, Y. Bengio, and P. Haffner, “Gradient-based learning applied to document recognition,” *Proceedings of the IEEE*, vol. 86, no. 11, pp. 2278–2324, 1998. DOI: 10.1109/5.726791.
- [28] Y. LeCun, Y. Bengio, and G. Hinton, “Deep learning,” *nature*, vol. 521, no. 7553, pp. 436–444, 2015. DOI: 10.1038/nature14539.
- [29] A. Krizhevsky, I. Sutskever, and G. E. Hinton, “Imagenet classification with deep convolutional neural networks,” in *Advances in neural information processing systems*, vol. 25, 2012, pp. 1097–1105. DOI: 10.1145/3065386.
- [30] N. Tajbakhsh, J. Y. Shin, S. R. Gurudu, R. T. Hurst, C. B. Kendall, M. B. Gotway, and J. Liang, “Convolutional neural networks for medical image analysis: Full training or fine tuning?” *IEEE Transactions on Medical Imaging*, vol. 35, no. 5, pp. 1299–1312, 2016. DOI: 10.1109/TMI.2016.2535302.
- [31] L. Jin, F. Wang, and Q. Yang, “Performance analysis and optimization of permanent magnet synchronous motor based on deep learning,” in *2017 20th International Conference on Electrical Machines and Systems (ICEMS)*, 2017, pp. 1–5. DOI: 10.1109/ICEMS.2017.8056321.
- [32] C. Gletter, A. Mayer, J. Kallo, T. Winsel, and O. Nelles, “A novel approach for development of neural network based electrical machine models for hev system-level design optimization.,” in *VEHITS*, 2019, pp. 17–24. DOI: 10.5220/0007570300170024.
- [33] A. Khan, V. Ghorbanian, and D. Lowther, “Deep learning for magnetic field estimation,” *IEEE Transactions on Magnetics*, vol. 55, no. 6, pp. 1–4, 2019. DOI: 10.1109/TMAG.2019.2899304.
- [34] W. Kirchgässner, O. Wallscheid, and J. Böcker, “Deep residual convolutional and recurrent neural networks for temperature estimation in permanent magnet synchronous motors,” in *2019 IEEE International Electric Machines Drives Conference (IEMDC)*, 2019, pp. 1439–1446. DOI: 10.1109/IEMDC.2019.8785109.
- [35] Y. Li, T. Sun, W. Zhang, S. Li, J. Liang, and Z. Wang, “A torque observer for ipmsm drives based on deep neural network,” in *2019 14th IEEE Conference on Industrial Electronics and Applications (ICIEA)*, 2019, pp. 1530–1535. DOI: 10.1109/ICIEA.2019.8834195.
- [36] H. Sasaki and H. Igarashi, “Topology optimization of ipm motor with aid of deep learning,” *International Journal of Applied Electromagnetics and Mechanics*, vol. 59, no. 1, pp. 87–96, 2019. DOI: 10.3233/JAE-171164.
- [37] S. Doi, H. Sasaki, and H. Igarashi, “Multi-objective topology optimization of rotating machines using deep learning,” *IEEE Transactions on Magnetics*, vol. 55, no. 6, pp. 1–5, 2019. DOI: 10.1109/TMAG.2019.2899934.
- [38] A. Khan, M. H. Mohammadi, V. Ghorbanian, and D. Lowther, “Efficiency map prediction of motor drives using deep learning,” *IEEE Transactions on Magnetics*, vol. 56, no. 3, pp. 1–4, 2020. DOI: 10.1109/TMAG.2019.2957162.

- [39] Y. Yongmin, “Multi-objective optimal design of permanent magnet synchronous motor for electric vehicle based on deep learning,” *Applied Sciences*, vol. 10, p. 482, Jan. 2020. DOI: 10.3390/app10020482.
- [40] S. Barmada, N. Fontana, L. Sani, D. Thomopoulos, and M. Tucci, “Deep learning and reduced models for fast optimization in electromagnetics,” *IEEE Transactions on Magnetics*, vol. 56, no. 3, pp. 1–4, 2020. DOI: 10.1109/TMAG.2019.2957197.
- [41] D.-A. Clevert, T. Unterthiner, and S. Hochreiter, “Fast and accurate deep network learning by exponential linear units (elus),” in *ICLR 2016 : International Conference on Learning Representations 2016*, 2016.
- [42] D. E. Rumelhart, G. E. Hinton, and R. J. Williams, “Learning representations by back-propagating errors,” *nature*, vol. 323, no. 6088, pp. 533–536, 1986. DOI: <https://doi.org/10.1038/323533a0>.
- [43] D. P. Kingma and J. L. Ba, “Adam: A method for stochastic optimization,” in *International Conference on Learning Representations (ICLR 2015)*, 2015.
- [44] M. Abadi, A. Agarwal, P. Barham, E. Brevdo, Z. Chen, C. Citro, G. S. Corrado, A. Davis, J. Dean, M. Devin, S. Ghemawat, I. Goodfellow, A. Harp, G. Irving, M. Isard, Y. Jia, R. Jozefowicz, L. Kaiser, M. Kudlur, J. Levenberg, D. Mané, R. Monga, S. Moore, D. Murray, C. Olah, M. Schuster, J. Shlens, B. Steiner, I. Sutskever, K. Talwar, P. Tucker, V. Vanhoucke, V. Vasudevan, F. Viégas, O. Vinyals, P. Warden, M. Wattenberg, M. Wicke, Y. Yu, and X. Zheng, *TensorFlow: Large-scale machine learning on heterogeneous systems*, 2015. [Online]. Available: <https://www.tensorflow.org/>.
- [45] ISO Guide, “Guide to the expression of uncertainty in measurement,” *International Standard Organisation, Geneva*, 1993.
- [46] “Pearson’s correlation coefficient,” in *Encyclopedia of Public Health*, W. Kirch, Ed. Dordrecht: Springer Netherlands, 2008, pp. 1090–1091, ISBN: 978-1-4020-5614-7. DOI: 10.1007/978-1-4020-5614-7_2569.
- [47] C. E. Rasmussen and C. K. I. Williams, *Gaussian Processes for Machine Learning (Adaptive Computation and Machine Learning)*. The MIT Press, 2006, pp. 7–30, ISBN: 026218253X. [Online]. Available: <http://www.gaussianprocess.org/gpml/>.
- [48] F. Pedregosa, G. Varoquaux, A. Gramfort, V. Michel, B. Thirion, O. Grisel, M. Blondel, P. Prettenhofer, R. Weiss, V. Dubourg, J. Vanderplas, A. Passos, D. Cournapeau, M. Brucher, M. Perrot, and É. Duchesnay, “Scikit-learn: Machine learning in python,” *Journal of Machine Learning Research*, vol. 12, no. 85, pp. 2825–2830, 2011.
- [49] L. Buitinck, G. Louppe, M. Blondel, F. Pedregosa, A. Mueller, O. Grisel, V. Niculae, P. Prettenhofer, A. Gramfort, J. Grobler, R. Layton, J. VanderPlas, A. Joly, B. Holt, and G. Varoquaux, “API design for machine learning software: Experiences from the scikit-learn project,” in *ECML PKDD Workshop: Languages for Data Mining and Machine Learning*, 2013, pp. 108–122.
- [50] R. H. Byrd, P. Lu, J. Nocedal, and C. Zhu, “A limited memory algorithm for bound constrained optimization,” *SIAM Journal on Scientific Computing*, vol. 16, no. 5, pp. 1190–1208, 1995. DOI: 10.1137/0916069.
- [51] J. L. Morales and J. Nocedal, “Remark on “algorithm 778: L-bfgs-b: Fortran subroutines for large-scale bound constrained optimization”,,” *ACM Trans. Math. Softw.*, vol. 38, no. 7, Dec. 2011, ISSN: 0098-3500. DOI: 10.1145/2049662.2049669.

...